International Journal of u- and e- Service, Science and Technology
Vol.8, No.1 (2015), pp.311-322
http://dx.doi.org/10.14257/ijunesst.2015.8.1.28

Research on Electromagnetic and Dynamic Properties of LPMBLDCM for Electromagnetic Launch

Huilai Li and Xiaomin Li

Shijiazhuang Mechanical Engineering College, Shijiazhuang, Hebei, 050003, China
lihuilai37@126.com

Abstract

In order to improve the thrust characteristics of moving-magnet type linear permanent magnet brushless DC motor (LPMBLDCM), the structural characteristics and magnetic field are analyzed. The influence of electrical parameters and structural parameters on the electromagnetic properties and thrust performance are researched by finite element analysis (FEA). The cogging force, back electromotive force (back-EMF), air-gap magnetic field distribution, mover velocity as well as thrust output are studied by taking some practical parameters into account, including pole/arc coefficient, air-gap width, voltage and current. The LPMBLDCM system is established, and some relevant tests are taken to verify the simulation results. Simulation and experimental results show that the thrust and mover velocity are mainly affected by some key parameters. The results will surely provide the reference and guidance for the optimization of electromagnetic and thrust characteristics of LPMBLDCM.

Keywords: *LPMBLDCM; structural parameters; electrical parameters; velocity; thrust*

1. Introduction

Linear permanent magnet brushless DC motor (LPMBDCM) has the advantage of high flux density, large thrust, high energy efficiency and simple structure, which is very suitable to be applied to UAV launch for electromagnetic catapult[1-2]. Different with the chemical launcher, linear motor for electromagnetic launch generally require high voltage, high current, high and constant thrust. The variation range of transient velocity for mover is very large, and the terminal velocity can reach several tens meters per second. All those special conditions require high thrust output and energy efficiency for LPMBDCM. Therefore, the research of structural parameters and electrical parameters effect rule are necessary to promote performance for LPMBDCM design.

The optimization design of structural parameters and back-EMF waveforms are two main ways to promote thrust performance for LPMBDCM. The research of single structural parameters to improve the performance concerns pole/arc coefficient, slot width, thickness of iron yoke, winding mode, poles structure. However, this optimization method has its shortage. For the other non-objective parameters, they can't be optionally changed in simulated process. It must be recalculated when other parameters have been changed. The influences of gap length, thickness of magnet, pole arc coefficient, number of pole pairs to the average thrust have been already discussed for a double-sided linear synchronous motor used for electromagnetic catapults in [3], and some results are consistent with the computed results in [4]. However, it was found in [5] that the optimization of structural parameter can promote the velocity and thrust properties, in which the essence problem is the elimination of higher harmonics in the

ISSN: 2005-4246 IJUNESST

air gap flux density. For LPMBLDCM, the optimization of structural parameters can increase the flat width of trapezoidal back-EMF, so the thrust output will be smooth [6]. Generally speaking, the influences of structural parameters and electrical parameters on thrust performance are the same in outward form but different in essence. The former can promote the electromagnetic property to generate higher thrust; while the latter will increase the system efficiency through the electrical parameter matching [7-8].

In this paper, the influence of structural parameters and electrical parameters to the thrust performance for LPMBLDCM are investigated by simulation and experiment, which provide foundation for optimal design. The parameter matching and optimizing design problem for LPMBLDCM are explored to apply small and middle scale UAV launcher, and also to provide references to catapult design.

2. Magnetic Field Model Analysis

Fig. 1 shows the simplified diagram of two dimensional solution areas for LPMBLDCM. To calculate the flux density in the air-gap, the symmetry boundary conditions between permanent magnet is set to the model. The permanent magnet region, air-gap region, and slotted stator region are divided in turn along the *y*-axis direction with three boxes alveolar layers boundary. The moving-magnet mover could only slip along *x*-axis direction.

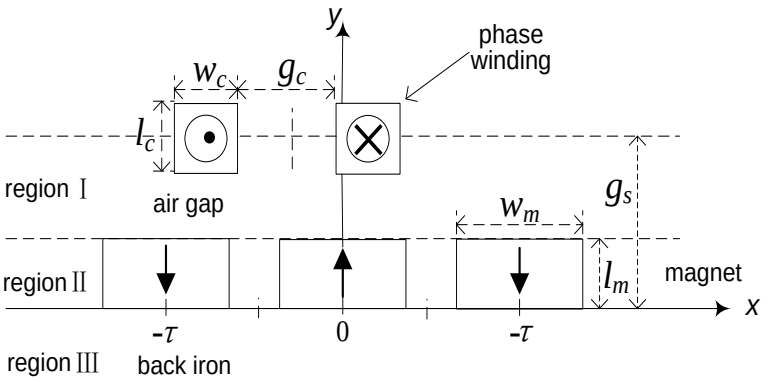

Figure 1. The Diagram of Two Dimensional Solution Area

According to Figure 1, assumption that (I) the stator is infinitely long in the *x*-direction; (ii) the current is injected only along *z*-direction; (iii) the permeability of the back iron is infinite[9]. The distribution equations of magnetic field for each layer are given as follows [10]:

$$\begin{cases} \dfrac{\partial^2 A_{\mathrm{I}}}{\partial x^2}+\dfrac{\partial^2 A_{\mathrm{I}}}{\partial y^2}=0 \qquad Regin\,\mathrm{I} \\ \dfrac{\partial^2 A_{\mathrm{II}}}{\partial x^2}+\dfrac{\partial^2 A_{\mathrm{II}}}{\partial y^2}=jv_x\dfrac{\pi}{\tau}(n-1)\sigma_m\mu_m A_{\mathrm{II}}-\mu_0 J_m \qquad Regin\,\mathrm{II} \\ \dfrac{\partial^2 A_{\mathrm{III}}}{\partial x^2}+\dfrac{\partial^2 A_{\mathrm{III}}}{\partial y^2}=jv_x\dfrac{\pi}{\tau}(n-1)\sigma_s\mu_s A_{\mathrm{III}} \qquad Regin\,\mathrm{III} \end{cases} \tag{1}$$

where A is the curl of magnetic vector; σ_s and σ_m respectively denotes the conductivity of permanent magnet and iron yoke; τ denotes the pole pitch; v_x denotes the mover velocity in the x-axis direction; n is the multiple of the space harmonics to fundamental field. J_m is derived from the formula (2).

$$J_m = \nabla \times M \tag{2}$$

where M is the magnetization characteristic of PM, and it can be written as the Fourier series about the x displacement.

$$M = \sum_{n=1,3,5,\cdots}^{\infty} \frac{4}{n\tau\pi} \frac{B_r}{\mu_m} \sin\left(\frac{\alpha n\pi}{2}\right) \cos\left(\frac{n\pi}{2} x\right) \tag{3}$$

where B_r is the residual magnetic flux density, μ_m is the relative permeability, α is the pole arc coefficient and τ is the pole pitch. Hence, A can be determined. The corresponding general solutions of Eqs.(1) are then given as:

$$\begin{cases} A_{\mathrm{I}} = \sum\limits_{n=-\infty, v1=1+2mqn}^{\infty} \{A\sinh(v_1 ay) + B\cosh(v_1 ay)\} \cdot e^{j(\omega_0 t - v_1 ax)} \\ A_{\mathrm{II}} = \sum\limits_{n=-\infty, v1=1+2mqn}^{\infty} \{C\sinh(a_m y) + D\cosh(a_m y)\} \cdot e^{j(\omega_0 t - v_1 ax)} - (B_r / a) e^{j(\omega_0 t - ax)} \\ A_{\mathrm{III}} = \sum\limits_{n=-\infty, v1=1+2mqn}^{\infty} \{E\sinh(a_s y) + F\cosh(a_s y)\} \cdot e^{j(\omega_0 t - v_1 ax)} \end{cases} \tag{4}$$

where $a = \pi / \tau$, $a_s = v_1 a \cdot \sqrt{1 + j\mu_s \sigma_s \omega_e / (v_1 a)^2}$ and $a_m = v_1 a \cdot \sqrt{1 + j\mu_m \sigma_m \omega_e / (v_1 a)^2}$.

Obtained the magnetic vector A and current density J, according to Ampere's law, the mover thrust can be estimated as formula (5).

$$\vec{F} = \int_V J \times B dV = \int_V J \times \left(i \frac{\partial A}{\partial x} + j \frac{\partial A}{\partial x} \right) dV \tag{5}$$

3. Finite Element Analysis and Results

3.1. Model Analysis and Parameter Settings

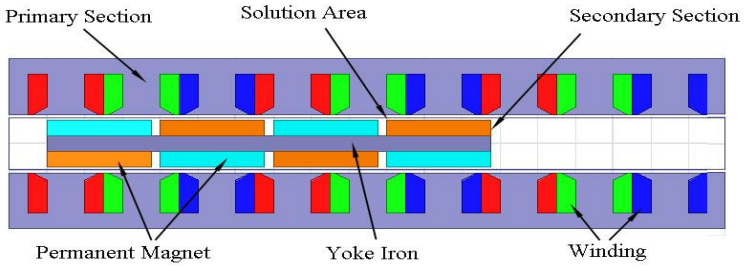

Figure 2. Dynamic Simulative Model of LPMBDCM

The transient process of electromagnetic launch is a highly coupled process. The dynamic process of electromagnetic launch for LPMBLDCM is researched using Maxwell Ansoft 2-D transient solver, which could solve the problem of direct calculation. Figure 2 shows the

simulation model of LPMBDCM, including mover, stator, winding, translation domain and solution domain. The current in the winding is added by external drive circuit, and the voltage and resistance values can be set as required. The simulation time is from 0 ms to 150 ms with 0.05 ms step-size change. The pole pitch (τ), length of air-gap (g_s), size of slot dimension (w_c, l_c, h_s), size of PM dimension (w_m, l_m, h_m), and the length of primary and secondary section should be adjusted properly. Some motor parameters and PM characteristic have been shown in Table Ⅰ.

Table 1. Motor Design Data and PM Characteristic

Symbol	*Item*	*Value*
τ	pole pitch	60mm
g_s	length of air-gap	2mm
z	slot number	45
w_c	width of slot	15mm
l_c	length of slot	20mm
h_s	depth of slot	100mm
w_m	width of PM	50mm
l_m	length of PM	90mm
h_m	thickness of PM	12mm
L_p	primary length	1.8m
L_s	secondary length	235mm
PM	material	Nd-Fe-B

3.2. Structural Parameters Effect and Its Analysis

3.2.1. A. The Influence of Pole/Arc Coefficient: For LPMBLDCM, the pole/arc coefficient is defined as:

$$\alpha = w_m / \tau \tag{6}$$

The magnetic permeability of PM is equal with that of air, so the flux density of air-gap is given as formula (7).

$$B(x,\alpha) = B_r(x)\frac{h_m}{h_m + g(x,a)} \tag{7}$$

where $B_r(x)$ is the remnant magnetism of PM, $g(x,a)$ is the distribution of available air-gap length, h_m is the length of PM magnetization direction. Assumption that the end-effect is neglected. The proposed linear motor moves x straight distance, which equate to $2\pi x / c$ angle for the rotating motor. So the cogging force for slot type motor can be written as follow [11].

$$F_{cog} = \frac{\pi^2 zd}{4\mu_0}\left(\frac{L_p}{\pi} g_s + g_s^2\right)\sum_{i=1}^{\infty} nG_n B_{r(nz/2p)} \sin\left(\frac{2\pi nz}{L_p} x\right) \tag{8}$$

where z is the slot number, p is the number of pole-pairs, $n = 2p / GCD(z, 2p)$.

The flat top width of back-EMF with different pole/arc coefficients are shown in Table Ⅱ.

Table 2. The Flat Top Width of Back-EMF with Different Pole/arc Coefficients

Pole/arc *coefficient*	Flat top width of back-EMF (degree)
0.65	108
0.75	116
0.85	120
0.95	122

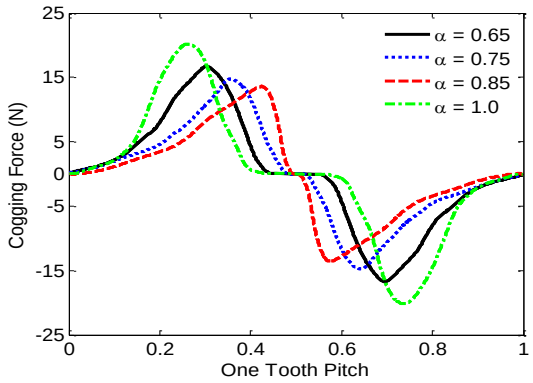

Figure 3. The Cogging Force with Different Pole/arc Coefficient on One Tooth Pitch

The cogging force with different pole/arc coefficient on one tooth pitch has been obtained, as shown in Figure 3. It can be seen from the figure that the cogging force on one tooth pitch appears to decrease with the increase of pole/arc coefficient. While α is approximate to 1, yet the cogging force will become large. When $\alpha = 1$, the cogging force is much larger than that of with the other value. The peak of cogging force appears at some special locations on one tooth pitch, and it presents a cyclical changes. So the cogging force will be evidently decreased with the suitable pole/arc coefficient.

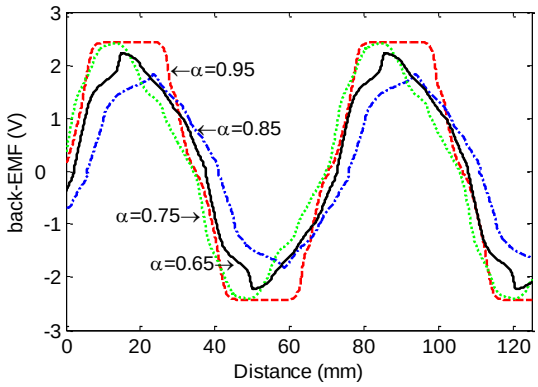

Figure 4. The Back-EMF Curve with Different Air-gap Width

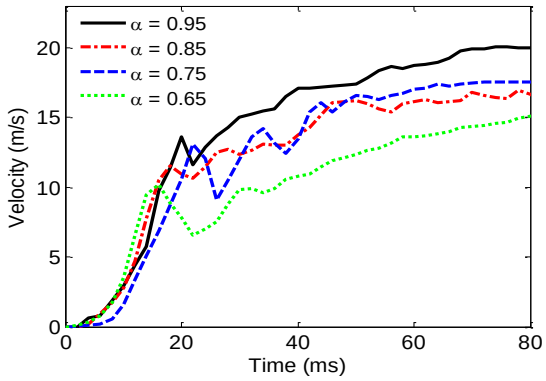

Figure 5. Result of Acceleration Considering Pole/Arc Coefficient

Figure 4 shows the idle back-EMF curve for LPMBLDCM with different pole/arc coefficient, when the constant mover velocity is 2 m/s. Figure 5 gives the acceleration change for LPMBLDCM with different pole/arc coefficient. Combined Figure 4 with Figure 5, it can be seen that the top width of back-EMF will become narrow down and the raised amplitude distortion will also appear with the decrescence of pole/arc coefficient. When $\alpha = 0.95$, the largest flat top width of back-EMF occurs with a 122 degree angle; when α is approximate to 1, the back-EMF curve presents trapezoidal wave. When α gradually decreases from 0.95 to 0.65, the back-EMF curve presents sinusoidal wave. The mover has different acceleration response when α respectively assumed at 0.65, 0.75, 0.85 and 0.95. The optimal acceleration response occurs while α is approximate to 0.75.

3.2.2. The Influence of Air-gap Width: The air-gap magnetic field for surface-mounted permanent magnet motor can be derived from the formula (2) as follow [12-13]

$$\begin{cases} B_{a\mathrm{I}\ y} = -\mu_0 \dfrac{\partial A_{\mathrm{I}}}{\partial y_1} = \dfrac{4B_r}{\pi} \times \sum\limits_{n=1,3,5}^{\infty} \dfrac{\sin(n\pi a_1)\sinh(n\pi h_1)\cos(n\pi(h_1+g_1-y_1))\cos(n\pi x_1)}{n\sinh(n\pi(g_1+h_1))} \\ B_{a\mathrm{II}\ y} = -\mu_0 \dfrac{\partial A_{\mathrm{II}}}{\partial y_1} + \mu_0 M = \dfrac{4B_r}{\pi} \times \sum\limits_{n=1,3,5}^{\infty} \dfrac{\sinh(n\pi(g_1+h_1)) - \sinh(n\pi g_1)\cosh(n\pi y_1)}{n\sinh(n\pi(g_1+h_1))} \sin(n\pi a_1)\cos(n\pi x_1) \end{cases} \tag{9}$$

where $x_1 = x/\tau$, $y_1 = y/\tau$, $h_1 = h_m/\tau$, $g_1 = g_s/\tau$ and $\alpha_1 = \alpha/\tau$.

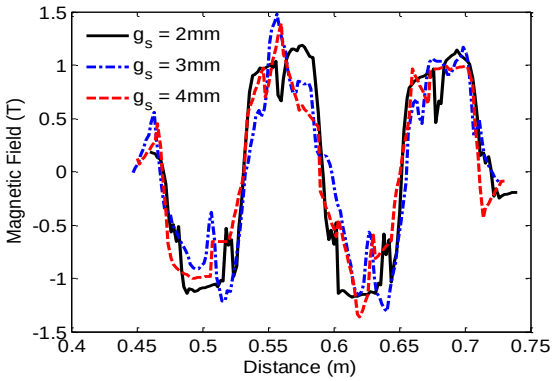

Figure 6. The Available Flux Density Curve with Different Air-gap Width

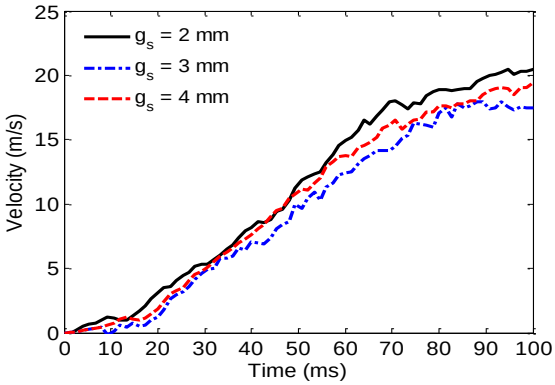

Figure 7. Results of Acceleration Considering Air-gap Width

Figure 6 shows the available flux density curve with different air-gap width. The mover accelerations are presented with different air-gap width, as shown in Figure 7. The selected air-gap widths are 2 mm, 3 mm and 4mm for LPMBLDCM model. Figure 6 and Figure 7 show that the trapezoidal flat top is evident when the air-gap width is 2 mm. But there is a small hollow on the flat top. This decayable field occurs mainly caused by slot effect. As the air-gap width increases, the air-gap magnetic field decreases and occurs clutter. The short air-gap width can lead the better acceleration performance, but this will generate the larger normal magnetic pull to eliminate. The obvious acceleration starts from 0 ms to 60 ms, and the acceleration appears a gradual rolloff until to zero. The acceleration will not increase after 100 ms.

3.3. Electrical Parameters Effect and Its Analysis

Figure 8 shows the velocity acceleration considering actuating voltage from 60 V to 240 V. It can be seen from Fig. 8 that the transient acceleration response does not show linear rule with the increase of voltage. The acceleration evidently presents increasing at first and then decrease to zero in the process. When the voltage exceeds 180 V, the thrust in the x-axis direction and mover acceleration will increase slowly. The thrust fluctuation appeared during the transient start procedure and this can be explained that the eddy current resistance makes the mover decelerate, which concerns with the change rate of coil current. The Ampere force still plays a dominative role in the start procedure, so the thrust increases with the enhancement of the voltage despite a little fluctuation associated.

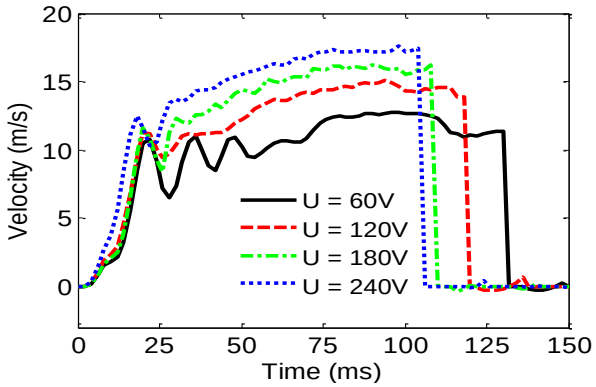

Figure 8. Results of Acceleration Considering Voltage

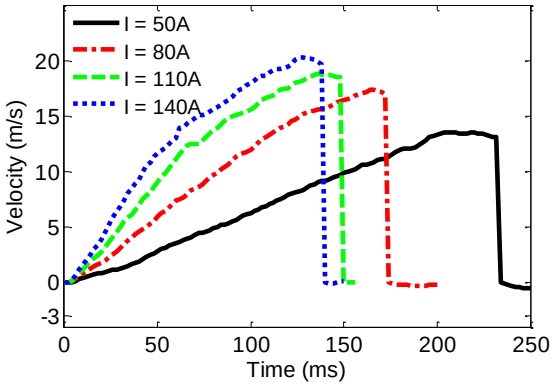

Figure 9. Results of Acceleration Considering Current

The mover acceleration under different actuating current is presented, as shown in Figure 9. The selected typical current values are 50 A, 80 A, 110 A and 140 A. With the enhancement of actuating current, the maximum velocity increases from 12.73 m/s to 19.52 m/s, when the actuating current is 50 A to 140 A. The mover velocity almost show linear relation when the number of ampere turns is below 400. This can be explained that the short air-gap will provided larger magnetic field density, which the mover velocity will become large and the acceleration time will also become short. The mover acceleration is not evident when the actuating current exceeds at given value, such as 200A for concerned model machine. The Ampere force can't increases linearly due to the saturated air-gap field. On the other hand, the force is decided by current, field and position according the Ampere's law, so the thrust doesn't increases linearly.

4. Experiment and Discussion

According to the schematic model, a subscale long primary LPMBDCM system is established, as shown in Figure 10.

Figure 10. Prototype Machine of a Subscale Long- primary LPMBDCM

Figure 11 shows the measured and simulated data for mover velocity and average thrust; when the voltage value changes from 48 V to 240 V. Simulation and experimental results obtained are shown in Table 3.

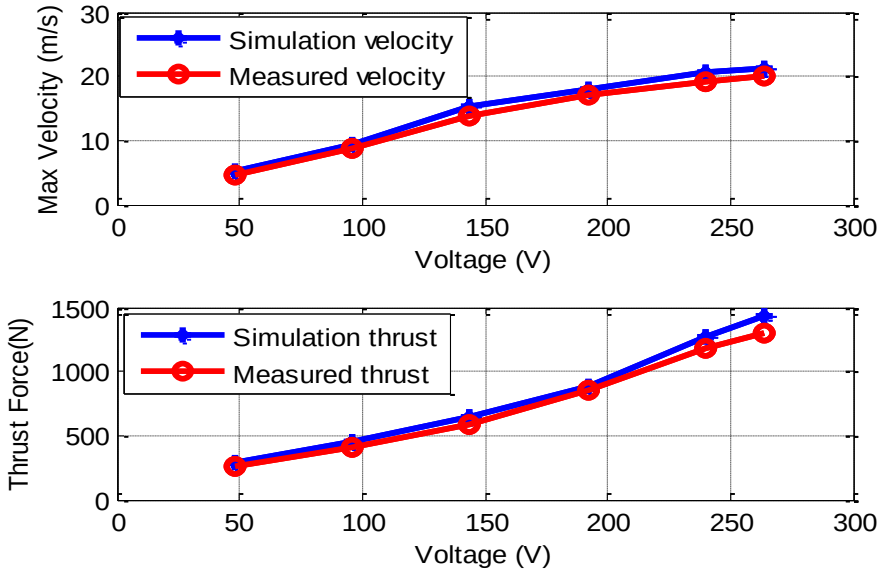

Figure 11. Measured and Simulated Mover Velocity and Average Thrust

Table 3. Experiment and Simulation Results for Thrust and Velocity

Voltage $U(V)$	48	96	144	180	216	240
Average simulation thrust (N)	288	446	639	883	1265	1432
Average measured thrust (N)	255	415	588	850	1186	1304
Max simulation velocity (m/s)	5.24	9.26	15.32	18.06	20.66	21.28
Max measured velocity (m/s)	4.95	8.84	13.85	17.09	19.25	20.06

Figure 11 and Table 3 show that the thrust output and mover velocity almost show linear accretion when the actuating voltage is blew 200V. With the increase of voltage, the thrust output and mover velocity do not appear exactly as a linear relation. The thrust output can't be continually promoted if the enhancement of the voltage. The variation rules obtained from the experiment and simulation results are basically consistent. The measured results are a little smaller than simulation results due to the sliding resistance, which verify the correctness of simulation analysis.

5. Conclusion

The influence of structural parameter and electrical parameter on electromagnetic and dynamic properties for LPMBLDCLM is the basic work for multi-parameter optimization design and segmented design. The theoretical working principle and magnetic field for LPMBDCM are analyzed in this paper. The influence of current and voltage as well as some structural parameters on electromagnetic properties and thrust performance for LPMBLDCM are researched by FEA and experiment. The results show that the optimal single pole/arc coefficient is 0.75 and the appropriate air-gap width for proposed 1.8m LPMBLDCM can be designed as 3mm. The enhancement of actuating voltage can apparently increase the mover velocity when the voltage is less than 200V.

The proposed LPMBLDCM has the capacity of 17 m/s mover velocity and 1400 N thrust output with 10 kg load when the voltage is 240 V. Simulation results in FEA model agree well with the measured results, which validates the analytical and simulatical model.

References

[1] M. R. Doyle, D. J. Samuel, T. Conway, and R. R. Klimowski. "Electromagnetic aircraft launch systems-EMALS," *IEEE Trans. Magn*., vol.31, NO 1, pp. 528–533 (**1995**).
[2] D Patterson, A Monti, C Brice and T Bertoncelli, "Design and simulation of an electromagnetic aircraft launch system", in 37th IAS Annu. Meeting, vol.3, pp. 1950–1957 (**2002**).
[3] Liyi Li, Ma Mingna, Baoquan Kou and Qingquan Chen. "Analysis and Design of Moving-Magnet-Type Linear Synchronous Motor for Electromagnetic Launch System", *IEEE Trans. Plasma Sci.*, vol.39, pp. 121–126 (**2013**).
[4] Kou Bao-Quan, Wu Hong-Xing, Li Li-Yi, Zhang Liang-Liang, Zhao Zhe, and Cao Hai-Chuan. "The Thrust Characteristics Investigation of Doubled-Side Plate Permanent Magnet Linear Synchronous Motor for EML", *IEEE Trans. Magn.*, vol.45, NO 1, pp.501–505 (**2009**).
[5] Seahn Oh, Seungjae Min, and Jung-Pyo Hong. "Air Gap Flux Density Waveform Design of Surface-Mounted Permanent Magnet Motor Considering Magnet Shape and Magnetization Direction". *IEEE Trans. Magn.*, vol.49, no 5, pp. 2393–2396 (**2013**).
[6] Yong Li, Jibin Zou, and Yongping Lu. "Optimum Design of Magnet Shape in Permanent-Magnet Synchronous Motors", *IEEE Trans. Magn.*, vol.39, NO.6, pp. 3523–3526 (**2003**).
[7] Ryohei Oishi, Satoshi Horima, Hiroya Sugimoto, and Akira Chiba. "A Novel Parallel Motor Winding Structure for Bearingless Motors". *IEEE Trans. Magn.*, vol.49, NO.5, pp. 2287–2290 (**2013**).
[8] Miroslav Markovic and Yves Perriard. "Optimization Design of a Segmented Halbach Permanent Magnet Motor Using an Analytical Model". *IEEE Trans. Magn.*, vol.45, NO.7, pp. 2955–2960 (**2009**).
[9] Junyong Lu, and Weiming Ma, "Research on end effect of linear induction machines for high speed industrial transportation," *IEEE Trans. Plasma Sci.*, vol. 39, pp. 116–120 (**2011**).
[10] K. Ng., Z. Q. Zhu and D. Howe. "Open-Circuit Field Distribution in a Brushless Motor with Diametrically Magnetised PM Motor, Accounting for Slotting and Eddy Current Effects", *IEEE Trans. Magn.*, vol.32, NO.5, pp. 5070–5072 (**1996**).
[11] Seyed Ehsan Abdollahi and Sadegh Vaez-Zadeh. "Reducing Cogging Torque in Flux Switching Motors With Segmented Rotor", *IEEE Trans. Magn.*, vol.49, NO.10, pp. 5304–5309 (**2013**).
[12] Qiu Zhijian, Li Chen, Zhou Xiaoyan, and Zhang Yuejin. "Analytical Calculation of No-Load Air-Gap Magnetic Field in Surface-Mounted Permanent Magnet Motors with Rotor Eccentricity", Transactions Of China Electrotechnical Society, vol.28, pp.114–120 (**2013**).
[13] LIU Shao-gang, QIU Bo. "Analytic analysis of air gap field of moving-magnet linear permanent magnet brushless DC motors", Electric Machines And Control, vol.13, pp.62–66 (**2009**).

Authors

Huilai Li, he received the B.S. degree in electrical engineering from the Xi'dian University, Xi'an, China, in 2008 and the M.S. degree from Mechanical Engineering College, Shijiazhuang, China, in 2010, where he is currently working toward the Ph.D. degree since the year of 2011. His research interests include permanent magnet linear motor and linear electromagnetic launch, and special type electronic machine design and its control.

Xiaomin Li, he received the B.S. degree in Mechanical Engineering College, and the M.S. and Ph.D.degree from Beijing University of Aeronautics and Astronautics, Beijing, China, in 1996 and 1999. He was with the Mobile Station for Postdoctoral Research Program in Institute of Acoustics from Chinese Academy of Sciences Beijing from 2000 to 2002. His research interests include application of navigation technology and high-speed data link control.